SAND2022-7441C

Grid-Forming Inverter's Capability to Support Dynamic Microgrids with High Penetrations of Photovoltaics Systems

Rachid Darbali-Zamora[1], C. Birk Jones[1] and Erick E. Aponte-Bezares[2]

[1]Sandia National Laboratories, Albuquerque, New Mexico, 87185, USA

[2]University of Puerto Rico-Mayagüez, Mayagüez, Puerto Rico 00682, USA

***Abstract* – Grid-forming (GFM) inverters that support photovoltaic (PV) and dynamic microgrids, that expand and contract depending on available resources, must adapt. Unlike common microgrid approaches, that require significant financial investments to maintain operations of a system of a set size, this approach provides necessary resilience for a critical load at a reduced cost. To work, a GFM inverter must maintain appropriate voltage and frequency as the magnitude of PV output and loads change quickly during a switching event that acts to reduce the difference between generation and consumption. The simulation effort, described here, studies the potential capabilities of the GFM to support variable PV generation and fast changes in the microgrid's size that either increase or decrease the systems size. Simulations in *MATLAB/Simulink* showed that a GFM inverter can maintain a frequency around 60 Hz and voltage between 0.995 pu and 1.005 pu during variable PV generation and when microgrids change their size by opening and closing switches in order to maintain balanced operations.**

Index Terms – photovoltaic inverter, grid-forming, distribution systems, circuit analysis, simulation, stability

I. Introduction

Unlike traditional photovoltaic (PV) inverters that operate as grid-following (GFL) devices, grid-forming (GFM) inverters control voltage and frequency at their point of common coupling (PCC) [1], [2]. GFM inverters support electric grids like synchronous generators (SG) but can operate using carbon free resources [3], such as battery energy storage systems. GFM inverters are anticipated to play a large role in ensuring stable operations of microgrids by providing frequency and voltage support. These GFM inverters allow for underserved communities, such as areas in Puerto Rico, to install and operate low-cost microgrids.

Development and testing of low-cost microgrid solutions is important since many vulnerable communities in Puerto Rico (and other regions of the U.S.) have suffered significantly in recent history. Two of the most notable natural disasters were Hurricane Irma and Maria, which struck the island of Puerto Rico in 2017 [4]. The combination of these two natural disasters caused loss of power resulting in the largest power outage in U.S. history [5], [6]. Even after the power was restored, the electrical systems throughout the island continued to experience outages, especially in rural and remote regions like Corcovada.

After the devastating 2017 hurricanes, Corcovada's water system was restored in a matter of hours because of an existing diesel generator that powered the 3.5 kW water pump. However, other critical and non-critical loads could not be served without the receiving power from the main grid. In 2015, a PV system was installed to operate the communities water pump. In the future, the critical water pump and other loads in the community can be powered during an outage without significant upgrades to the existing system using a GFM inverter.

To understand the GFM inverter's potential, this paper studies the operations of a GFM inverter inside a low-cost microgrid powering the water pump continuously as well as providing power to non-critical loads when distributed PV is able to support it. The administration of such a microgrid requires switching capabilities that will allow for the expansion and reduction of the system that optimally balance the load demand with power generation as conditions change throughout the day. An initial study found that this approach is possible using a Particle Swarm Optimization (PSO) [7]. To power the essential services, a GFM inverter, battery storage, and PV array are located at the critical load per the set up described in [8].

Initial studies, such as the PSO assessment of a "breathable" microgrid that expands and reduces its size as conditions change [7] or the inclusion of a distant PV array into a microgrid [8], assumed that the GFM inverter could maintain the microgrid's frequency and voltage during switching events. But a GFM inverter's specific capabilities for this type of dynamic microgrid switching operation has yet to be explored. This work, therefore, performs an advanced simulation of a potential microgrid in the rural community of Corcovada, Puerto Rico. The simulation effort emulated the GFM inverter, dynamic loads, GFL PV inverters, and electrical lines to provide an initial understanding of a GFM inverter's ability to support transitions in system size and PV availability.

This paper evaluates the integration of a GFM inverter in an isolated microgrid with a large penetration of GFL inverters scattered throughout the system. A dynamic *MATLAB/Simulink* model of an actual power distribution network based on community in Puerto Rico was created using local load data provided by the community and nearby irradiance profiles to emulate realistic operations. This meant that the irradiance profile includes variability, which is typical for Puerto Rico as rain clouds move into and through the mountainous regions in the afternoons.

The focus of this evaluation was on the GFM inverter's ability to support switching transitions intent on providing a more balanced system, and significant changes in PV power generation. Transient results for this application, which are unreported in existing literature, describe the frequency and voltage dynamics of the microgrid under varying configurations and conditions.

II. Distribution Feeder Model Description

Corcovada is a small community in the mountainous region of the municipality of Añasco, located to the West of Puerto Rico, with a population of 627 [2010]. This community has been operating their aqueduct system for 42 years.

In order to evaluate the dynamic switching microgrid, a simulation model of a distribution system representing the community was developed in *MATLAB/Simulink*. Fig. 1 illustrates the distribution feeders and the different switching group locations. The distribution feeder model consists of 50 buses, 48 distribution lines, 43 single-phase transformers, 14 single-phase GFL inverters, a three phase GFM inverter, 36 residential loads and a critical load representing the community water pump. Table I summarizes the switching group generation and load demand.

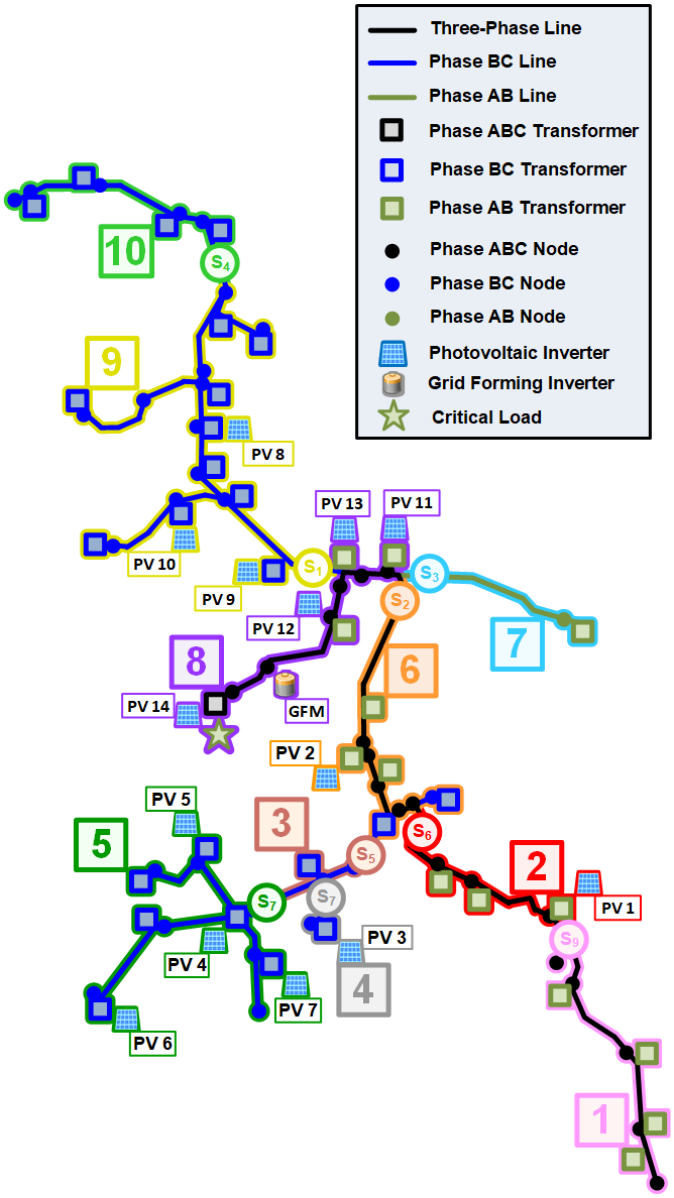

Fig. 1. Diagram of the Corcovada Distribution Feeder shows the lines phases, switching groups, PV locations, loads, and GFM inverter.

TABLE I:
MICROGRID SWITCHING GROUP DESCRIPTION

Switching Group	Photovoltaic Inverter			Total Load Demand	
	ID	Phases	Rating (kVA)	Active Power (kW)	Reactive Power (kVAR)
1	-	-	-	28.60	0.00
2	PV 1	AB	5.00	25.80	0.00
3	-	-	-	19.50	0.00
4	PV 3	BC	26.00	44.00	0.00
5	PV 4	BC	23.00	99.35	0.00
	PV 5	BC	5.00		
	PV 6	BC	10.00		
	PV 7	BC	44.00		
6	PV 2	AB	12.00	100.50	0.00
7	-	-	-	2.60	0.00
8	PV 11	AB	32.00	66.55	4.00
	PV 12	AB	5.00		
	PV 13	AB	8.00		
	PV 14	AB	21.00		
9	PV 8	BC	10.00	53.00	0.00
	PV 9	BC	6.50		
	PV 10	BC	4.50		
10	-	-	-	47.60	0.00
Total			**212.00**	**487.50**	**4.00**

The system is a portion of a larger feeder. Hence, the loads are only distributed throughout phases AB and BC, with no loads connected to phases AC. Moreover, there are no lines or transformers for phase AC. This caused a voltage imbalance in the system. The total peak load consumption of the microgrid is 487.50 kW. In addition to the residential loads, the community's 5 hp (3.7 kW) water pump serves as the critical load of the system, connected to phase AB. The total PV generation of the microgrid model is 191 kVA.

In addition to the household PV systems, the water pump has a dedicated PV system with a rated capacity of 21 kVA. The dynamic microgrid is divided into ten switching groups. Notice that some switching groups do not have PV generation. PV systems are located in switching groups 2, 4, 5, 6, 8 and 9. Switching group 8 is the nucleus of the dynamic microgrid, the critical load as well as a the GFM inverter. The 100 kVA GFM inverter is a three-phase inverter connected to switching group 8. Switching group 8 has a total load consumption of 66.5 kW and 4 kVAR, while there is a total of 66 kVA in GFL inverter power generation. During the dynamic microgrid group switching transitions, the total load consumption within the dynamic microgrid is 206.62 kW, while the total PV generation within the dynamic microgrid is 221.62 kW.

III. Distributed Energy Resource Modelling

Both GFL and GFM inverters models are tasked with generating power for the microgrid locally but also to safeguard coordinated continuous operations [10]. GFL inverters operate as current sources and following the grid voltage [11]. Multiple GFL inverter models are distributed throughout the microgrid system, as indicated in Fig. 1. GFM inverters define the reference voltage and frequency to ensure continuous operation of the community [12].

A. Grid-Following Inverter Model

To emulate the GFL inverter dynamics, a current controlled single-phase PV inverter model is implemented [13]. The GFL inverter model utilizes a Phase-Locked Loop (PLL) to synchronize to the grid [14]. Fig. 2 illustrates the block diagram for the GFL inverter model. In this diagram, the variable P_{ref} and Q_{ref} are the active and reactive power reference values. The active power is derived from a linear relationship to solar irradiance. The control is represented using the direct (d) and quadrature (q) axis reference frame, and a dq-current controller. Adjusting the d and q axis currents allows controlling both the active and reactive powers, respectively. The resulting equations for the total inverter active and reactive power injected to the grid using the *dq-fra*me are shown in equation (1) and equation (2), respectively.

$$P_{ref} = \frac{3}{2} \cdot \left(V_d \cdot I_d + V_q \cdot I_q\right) \qquad \#(1)$$

$$Q_{ref} = \frac{3}{2} \cdot \left(V_q \cdot I_d - V_d \cdot I_q\right) \qquad \#(2)$$

In these equations, the variables V_d and V_q are the d and q voltages in the *dq-frame*, respectively. The variables I_d and I_q are the d and q currents in the *dq-frame*, respectively. Table II summarizes the GFL inverter control parameters.

TABLE II:
GRID-FOLLOWING INVERTER PARAMETERS

Variable	*Description*	*Value*	*Unit*
Q_{ref}	*Reference Reactive Power*	0.00	*kVAR*
P_{ref}	*Reference Active Power*	5.00	*kW*
k_p	*Proportional Gain*	15.00	-
k_i	*Integral Gain*	200.00	-
f_o	*Grid Frequency*	60.00	*Hz*

A scaling method is used to calculate the controller and filter parameters for parallel-connected GFL inverters [15]. This scaling method is used to represent GFL inverters with different power ratings.

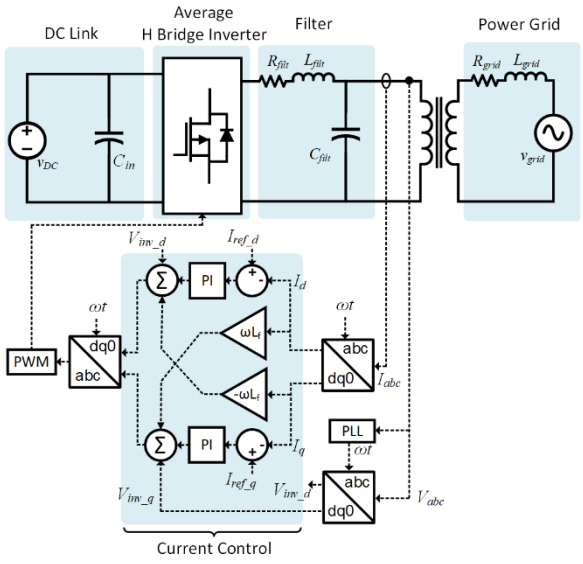

Fig. 2. Block Diagram Describing the dq-current controlled Single-Phase Grid-Following PV Inverter Control Scheme.

B. Grid-Forming Inverter Model

The dynamic behavior of a three-phase GFM inverter, is modeled using the Electric Reliability Technology Solutions (CERTS) control [16], [17], [18], [19]. Fig. 3 illustrates the block diagram for the CERTS GFM inverter model. The active power, reactive power, and voltage magnitude are calculated using the instantaneous values of the three-phase voltages and currents in the *αβ-frame*. Equation (3) through equation (5) are used to calculate P_o, Q_o, and V_m, respectively.

$$P_o = \frac{3}{2} \cdot \left(V_{g\alpha} \cdot I_{g\alpha} + V_{g\beta} \cdot I_{g\beta}\right) \qquad \#(3)$$

$$Q_o = \frac{3}{2} \cdot \left(V_{g\beta} \cdot I_{g\alpha} - V_{g\alpha} \cdot I_{g\beta}\right) \qquad \#(4)$$

$$V_m = \sqrt{v_{g\alpha}^2 + v_{g\beta}^2} \qquad \#(5)$$

In these equations, variables $v_{g\alpha}$, $v_{g\beta}$, $i_{g\alpha}$, and $i_{g\beta}$ are the *αβ-frame* voltages and currents, respectively. The active power/frequency droop control adjusts the frequency ω for the GFM inverter voltage. The variable m_p is the active power/frequency droop gain, P_{set} is the power setpoint, and ω_o represents the grid frequency. The reactive power/voltage droop control regulates the voltage of the GFM inverter. The variable V_{set} is the voltage setpoint. The modulation is calculated using a PI controller, where the variables k_{pv} and k_{iv} are the proportional and integral gains, respectively. Table III summarizes the GFM inverter control parameters.

TABLE III:
GRID-FORMING INVERTER PARAMETERS

Variable	*Description*	*Value*	*Unit*
V_{set}	*Voltage Setpoint*	1.00	*pu*
P_{set}	*Power Setpoint*	0.00	*pu*
m_p	*Active Power/Frequency Droop Gain*	3.77	*pu*
m_q	*Reactive Power/Voltage Droop Gain*	0.05	*pu*
k_{pv}	*Proportional Gain*	0.00	-
k_{iv}	*Integral Gain*	5.86	-
f_o	*Grid Frequency*	60.00	*Hz*

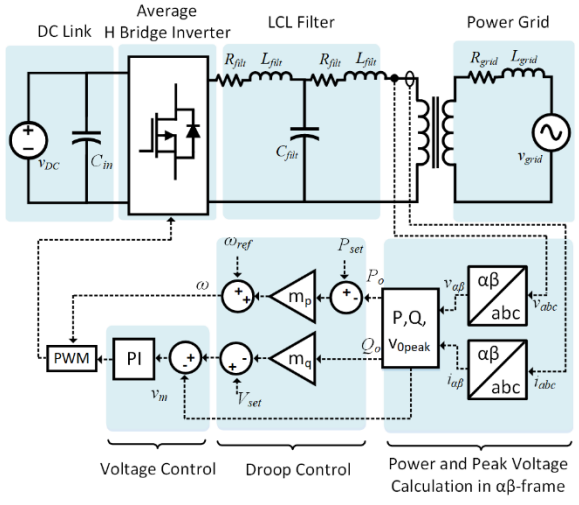

Fig. 3. Block Diagram Describing the CERTS Three-Phase Grid-Forming Inverter Control Scheme.

IV. Microgrid Switching Methodology

The simulations involved the operations of a changing microgrid supported by a GFM inverter. Throughout a single day of operations the microgrid expanded and reduced its size depending on the load demand and available PV power generation.

A. Microgrid Reconfiguration Approach

The switching control methodology considers an assessment and reconfiguration that includes monitoring of the system's performance as well as the modification of the switching states. Both the load consumption as well as the PV power generation from the microgrid and the aggregation of the net power for each switching group is monitored. The net power for each switching group and the system topology provides necessary inputs data for the PSO algorithm. The PSO algorithm processes the net power data and considers the topology of the microgrid to determine the new switching states. To determine the switching states, the PSO algorithm considers the overall topology and the location of the critical load. The solution obtained by the PSO algorithm is constrained to include the critical load switching group.

The reconfiguration optimization (that utilizes the PSO algorithm) determined the states for each switch, which defined the size of the microgrid, as described in [7]. The size of the microgrid depended on the optimization's ability to balance the system at different levels of PV power generation and load consumption. When a system was properly balanced, appropriate grid voltage level could be maintained. This will require that both the load consumption and PV power generation be as close as possible. The PSO algorithm minimizes the difference between load demand and PV power generation within the microgrid, as shown in equation (6).

$$\min_{P_l, P_g} \sum_{i=1}^{N} |P_l - P_g| \quad (6)$$

In this equation, the variable N is the number of iterations and the variables P_l and P_g are microgrid's load demand and power generation, respectively.

The objective of the PSO algorithm was constrained to only consider the switching group conditions that included the critical load. At the very least the microgrid included the critical load's switching group. At most, the optimization results could form a microgrid that included all the switching groups.

The optimization determined the best set of binary switching states that minimized this objective function within predetermined constraints. In this case, the number of particles was equal the number of switches, and the optimal switching configuration produced the smallest difference between load demand and PV power generation. This approach implemented the standard binary PSO algorithm to define the binary state for each switch. Initially, the algorithm set the particles to a random state; then at each iteration the particle state are updated based on two improved values. Finally, the velocity and position equations updated based on the two new values. The PSO algorithm considered all the neighboring switching groups to obtain the global minimum solution.

B. Expansion of the Microgrid

The expansion of the microgrid occurred when there was enough PV power generation to support a larger portion of the feeder's loads. During this type of event, the load increased from 94 kW to 203 kW, as depicted in Fig. 4. With the increase in switching groups, the PV power generation also increased to a maximum of 190 kW. However, because of the startup delay of the GFL inverters, it took 0.3 s after the expansion of the microgrid to reach the maximum PV power generation for the available irradiance.

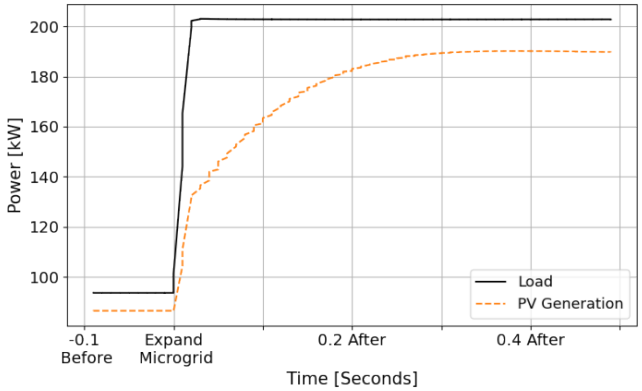

Fig. 4. To improve the balance between load consumption and PV power generation, the system expanded its boundaries to include more non-critical loads. Because of the start of delay of PV inverters, it took approximately 0.3 s for the generation to match closely with the load.

C. Reduction of the Microgrid

The reduction of the microgrid involved the opening of switches that excluded one or more switching groups from the microgrid. This reduced the load demand and the amount of PV power generation, as shown in Fig. 5. Notice from Fig. 5 that the load demand and PV power generation took 0.4 s after the reduction of the microgrid to reach a steady state. The PV power generation took a sharp drop in output when the system was reduced to 95 kW, which matched well with the load demand of 98 kW. However, the solar irradiance starts to decrease, which limited the output of the connected PV arrays.

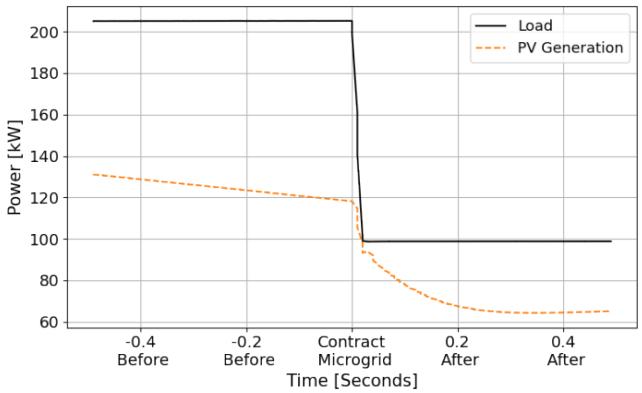

Fig. 5. A reduction in the system size occurs in order to improve the growing difference between load demand and PV power generation. In this case, a few seconds after the switching the active PV power generation.

V. MICROGRID SIMULATION

The *MATLAB/Simulink* model of Corcovada's electric power system was run for a single day of operations. The model considered the PSO switch states for each instance in time. It also used realistic irradiance and load profiles for the area, as shown in Fig. 6 and Fig. 7. Fig. 6 illustrates an example of an irradiance curve collected at the western region of Puerto Rico. Fig. 7 illustrates the total load demand profile used to represent the community residential household power consumption. Fig. 8 illustrates the active and reactive power demand of the community's critical load.

VI. SIMULATION RESULTS

The expansion and reduction of the dynamic microgrid, via optimized switching control, were supported by the GFM inverter. Sample maps of the dynamic microgrid around 11:00 AM and 4:00 PM are shown in Fig. 8. Between 11 AM and 11:10 AM the isolated electric grid experienced an expansion of its boundaries from four switch groups to eight. A second example shows the reduction in the microgrid's size from three switch groups at 3:40 PM to two at 4:00 PM. In both cases, the GFM inverter was able to supply the necessary active power and reactive power to support the microgrid's frequency and voltage. It also injected or absorbed reactive power needed to maintain proper voltage. The GFM inverter responded well to the change in system size and easily maintained the voltage and frequency around 1.0 pu and 60 Hz, respectively.

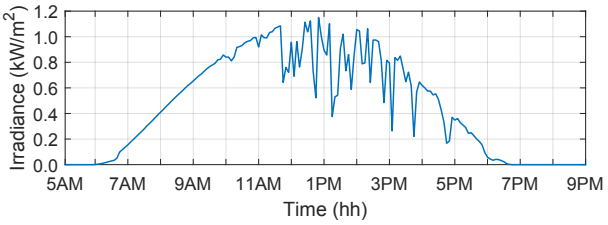

Fig. 6. Irradiance Profile from the Western Region of Puerto Rico.

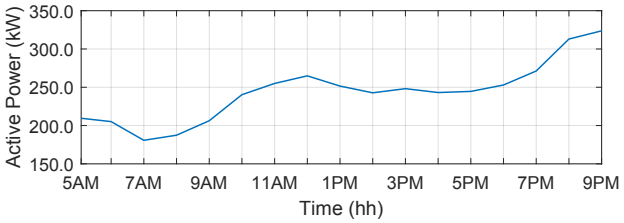

Fig. 7. Total Residential Load Demand Profile for the Community.

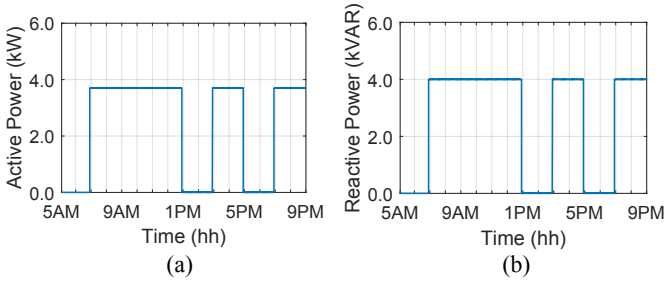

Fig. 8. Water Pump Critical Load Demand Profile. (a) Active Power. (b) Reactive Power.

Fig 9 illustrates an example of how the dynamic microgrid can change its switching states to either expand or reduce the size of the system.

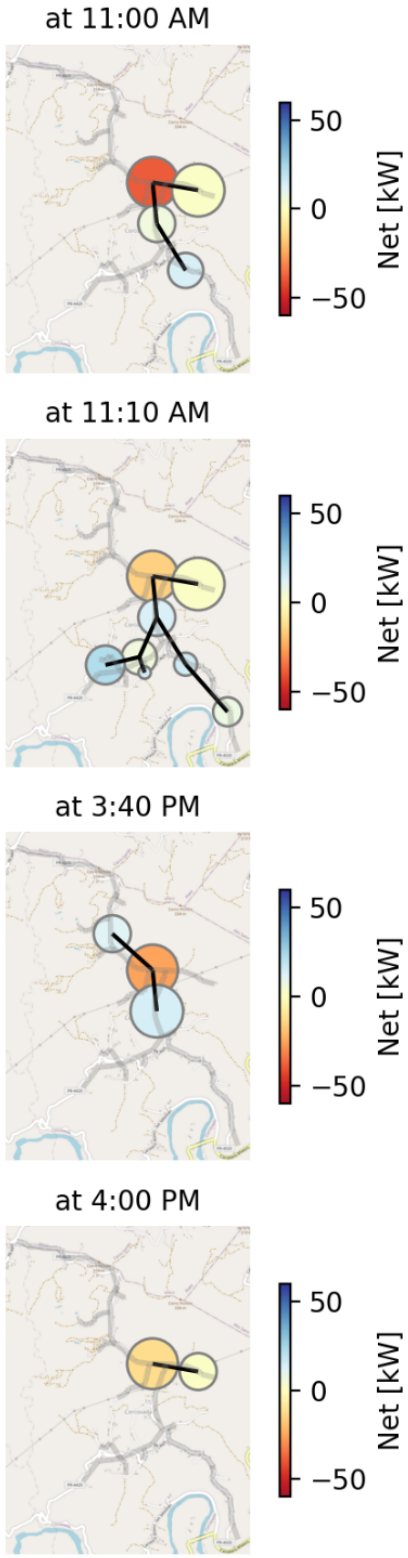

Fig. 9. Example operations of the dynamic microgrid show the reduction in the system size between 11:00 AM to 11:10 AM. At 3:40 PM the system powered three switch groups, which changed at 4:00 PM to include only two groups.

Fig. 10 illustrates the simulation results obtained for the total load demand and PV generation. Fig.11 illustrates the results for the per-phase voltage measured at the GFM inverter PCC. At the point, where the microgrid altered its boundaries by either increasing or decreasing its size, the voltage had noticeable deviations shown in plots in Fig. 11. However, in both situations, the GFM inverter's voltage did not change by more than 0.5%. Fig. 12 and Fig. 13 illustrate the power generation and load demand, RMS voltage and frequency during the microgrid expansion and reduction, respectively. When expanding the microgrid there was a frequency overshoot of less than 0.07% at most.

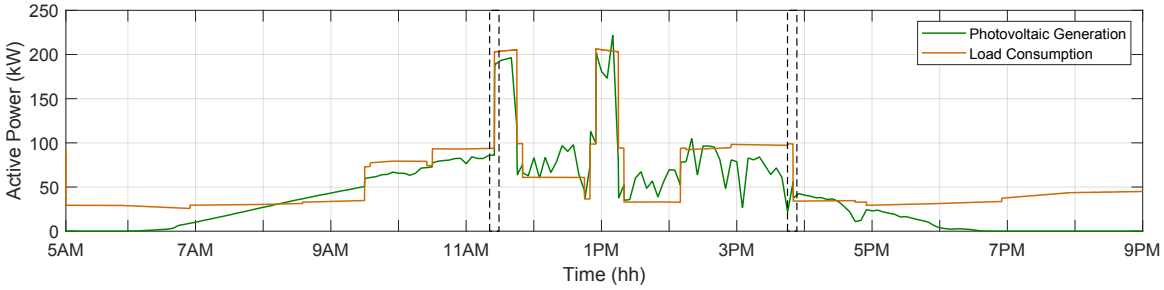

Fig. 10. Simulation Results for the Total Load demand and Generation within the Main Microgrid.

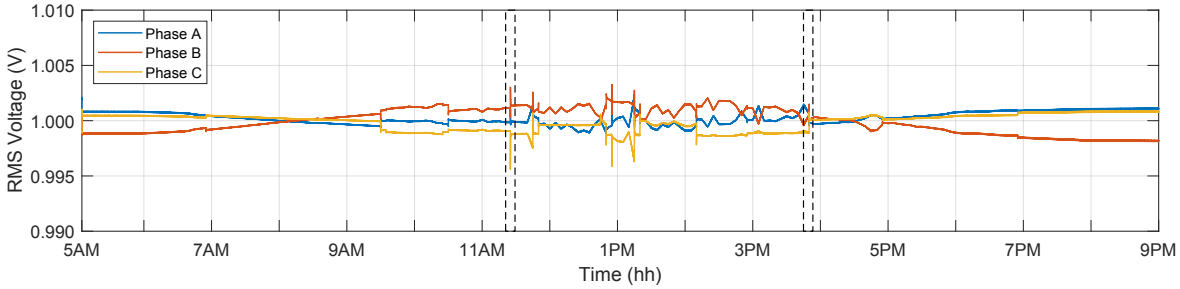

Fig. 11. Simulation Results for the GFM Inverters Phase Voltages During Switching Transitions.

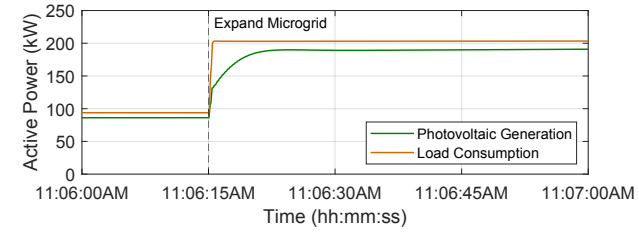

(a)

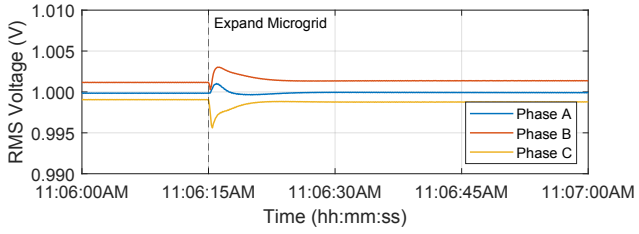

(b)

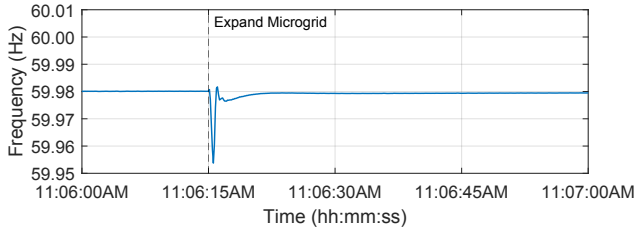

(c)

Fig. 12. Simulation results for the microgrid during an Expansion. (a) Generation Load. (b) Voltage. (c) Frequency.

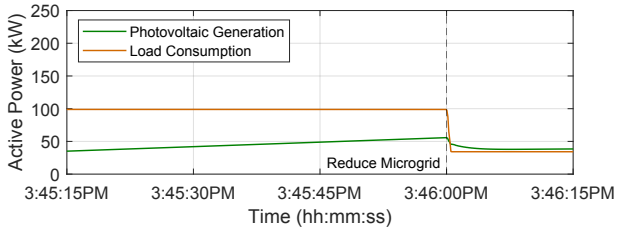

(a)

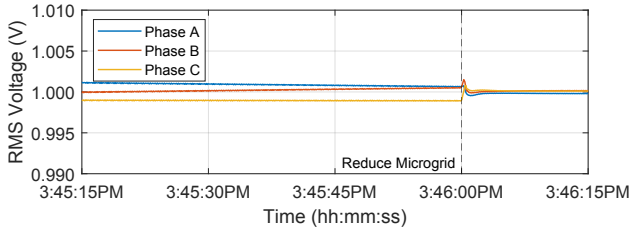

(b)

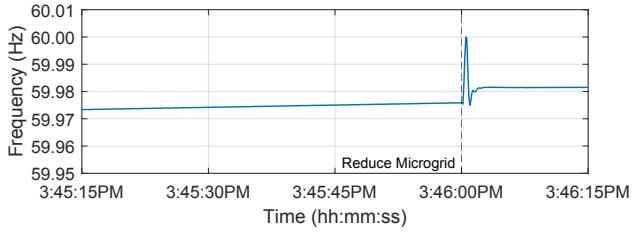

(c)

Fig. 13. Simulation results for the microgrid during a Reduction. (a) Generation Load. (b) Voltage. (c) Frequency.

Within the first seconds after the event, the load had reached its maximum. The PV on the other hand, took about 0.4 s to reach its maximum value. As a result, the voltage on each phase changed differently. Phase A voltage experienced a slight jump that reached a steady state about 0.2 s after the event. The other two phases took longer to reach steady state due to a more drastic change in power. The frequency had a noticeable dip in Fig. 12 of 0.05% before returning to the original value about 0.1 s since event. The reduction of the microgrid, intent on improving the load and generation balance, also resulted in minimal changes to the system voltage. Phase C experienced the largest change in voltage, as shown in Fig. 13 (b), of 0.063%. The other two phases had a decrease in voltage that returned to a steady state in 0.2 s after the event. The reduction in system size caused the frequency to increase by 0.28%.

Fig. 14 and Fig. 15 illustrate the simulation results for the per-phase active and reactive power of the GFM inverter, respectively. To manage the changes in load and PV generation, the GFM inverter altered its active and reactive power output. This is evident in Fig. 16 and Fig. 17 for the expansion and reduction cases, respectively. The microgrid is located at the very end of a very long feeder and the loads are connected not evenly distributed among the three phases. This caused an unbalance in the system. This imbalance is evident in the GFM inverter simulation results; each of the three phases have different active and reactive power behaviors.

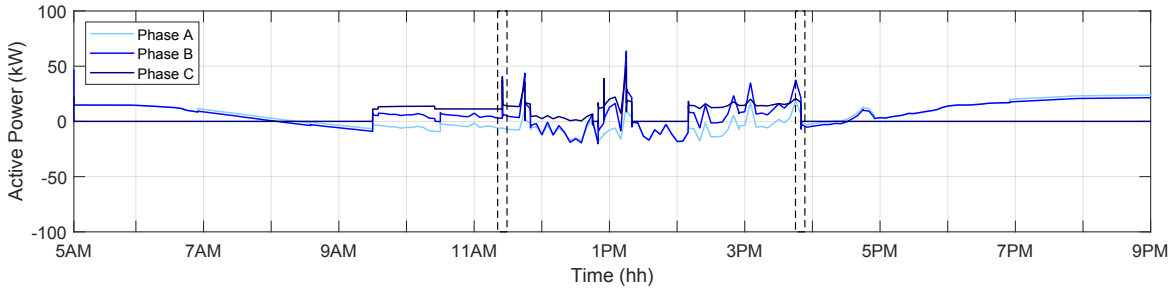

Fig. 14. Simulation Results for the GFM Inverters Active Power During Switching Transitions.

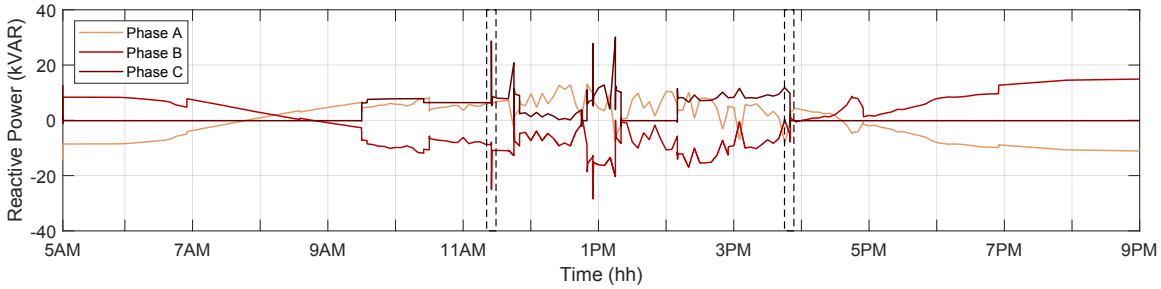

Fig. 15. Simulation Results for the GFM Inverters Reactive Power During Switching Transitions.

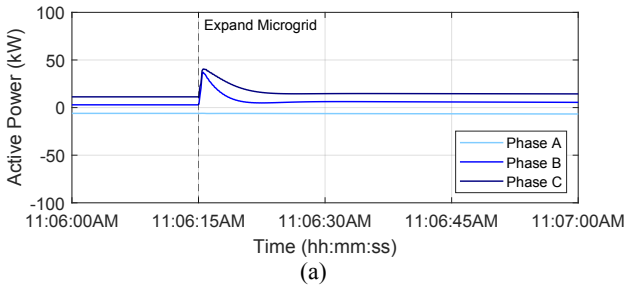

(a)

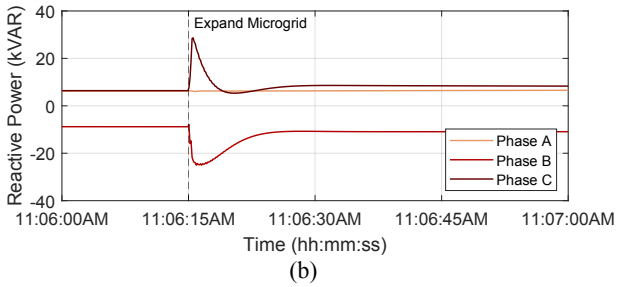

(b)

Fig. 16. Simulation results for the Microgrid During an Expansion. (a) Active Power. (b) Reactive Power.

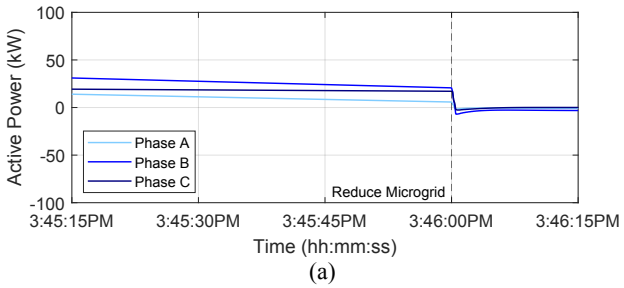

(a)

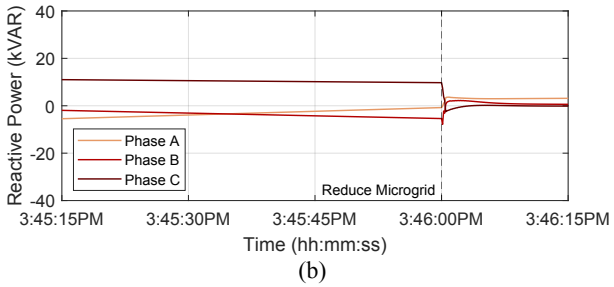

(b)

Fig. 17. Simulation results for the Microgrid During a Reduction. (a) Active Power. (b) Reactive Power.

Results from Fig. 16 illustrate that when the system expanded, the active power provided by the GFM inverter increased for Phases B and C. The active power provided by the GFM inverter did not change for Phase A. At the same time, reactive power was injected on Phase C, absorbed on Phase B, and remained a constant value on Phase A.

Fig. 17 shows that the active power for Phase B and C has similar behavior before and after the microgrid reduction. In this situation, Phase A active power did not remain constant and experienced a sudden drop of almost 10 kW. Prior to the event, The GFM inverter generated reactive power to Phase A, while absorbing reactive power from Phase B and C. Once the change in size occurred, reactive power was reduced to zero. The GFM inverter generated reactive power since the voltage was slightly below 1.0 pu. At the same time, the GFM inverter's reactive power on Phase B was negative in order to decrease the voltage.

VII. Conclusion

This paper presents integration of GFM inverters in a hypothetical, isolated dynamic microgrid with a large penetration of GFL inverters. A dynamic *MATLAB/Simulink* model based on an existing power distribution feeder is used to study the system performance. The simulation results were obtained for the entire microgrid, consisting of 10 switching groups. Dynamic simulation results are obtained for the GFM inverter operating under microgrid reconfiguration conditions. Varying irradiance data, collected from the West of Puerto Rico, was used for the GFL PV inverters. Varying load profiles were used to add more dynamic conditions. Microgrid reconfiguration controls were developed and successful used to determine when and what microgrids should be switched. The GFM inverter was able to support stable operations as the system changed its boundaries to either include or exclude loads and PV generation. Thus showing that dynamic operations is a viable solution for providing a low-cost, PV-based microgrid to remote communities.

Acknowledgement

Sandia National Laboratories is a multi-mission laboratory managed and operated by National Technology and Engineering Solutions of Sandia, LLC., a wholly owned subsidiary of Honeywell International, Inc., for the U.S. Department of Energy's National Nuclear Security Administration under contract DE-NA-0003525.

This material is based upon work supported by the U.S. Department of Energy's Office of Electricity under agreement with the FEMA. The authors acknowledge the leadership of the Corcovada Communal Committee Inc. NPO. They wholeheartedly collected data for this work and welcomed the authors into their community.

References

[1] P. P. Beires, C. L. Moreira and J. P. Lopes, "Grid-forming inverters replacing Diesel generators in small-scale islanded power systems", *IEEE Milan PowerTech*, 2019, pp. 1-6.

[2] B. K. Poolla, D. Groß and F. Dörfler, "Placement and Implementation of Grid-Forming and Grid-Following Virtual Inertia and Fast Frequency Response", *IEEE Transactions on Power Systems*, vol. 34, no. 4, pp. 3035-3046, July 2019.

[3] R. H. Lasseter, Z. Chen and D. Pattabiraman, "Grid-Forming Inverters: A Critical Asset for the Power Grid", *IEEE Journal of Emerging and Selected Topics in Power Electronics*, vol. 8, no. 2, pp. 925-935, June 2020.

[4] A. Kwasinski, "Effects of Hurricane Maria on Renewable Energy Systems in Puerto Rico", *7th International Conference on Renewable Energy Research and Applications (ICRERA)*, 2018, pp. 383-390.

[5] M. Gallucci, "Rebuilding Puerto Rico's Grid", *IEEE Spectrum*, vol. 55, no. 5, pp. 30-38, May 2018.

[6] C. Keerthisinghe, M. Ahumada-Paras, L. D. Pozzo, D. S. Kirschen, H. Pontes, W. K. Tatum, M. A. Matos, "PV-Battery Systems for Critical Loads During Emergencies: A Case Study from Puerto Rico After Hurricane Maria", *IEEE Power and Energy Magazine*, vol. 17, no. 1, pp. 82-92, Jan.-Feb. 2019.

[7] C. B. Jones, M.E. Ropp, J.H. Alvidrez, and R. Darbali-Zamora, "Optimized Control of Distribution Switches to Balance a Low Cost Photovoltaic Microgrid", *IEEE 48th Photovoltaic Specialists Conference (PVSC)*, 2021.

[8] C. B. Jones, M. Theristis, R. Darbali-Zamora, M. E. Ropp, M. J. Reno and M. Lave, "Switch Location Identification for Integrating a Distant Photovoltaic Array into a Microgrid", *IEEE Access*, 2022, pp. 1-12.

[9] M. Eriksson, M. Armendariz, O. O. Vasilenko, A. Saleem, and L. Nordström, "Multiagent-based distribution automation solution for self-healing grids", *IEEE Trans. Ind. Electron.*, vol. 62, no. 4, pp. 2620–2628, Apr. 2015.

[10] A. Singhal, T. L. Vu and W. Du, "Consensus Control for Coordinating Grid-Forming and Grid-Following Inverters in Microgrids", *IEEE Transactions on Smart Grid*, 2022, pp. 1-11.

[11] R. Darbali-Zamora, J. Johnson, N. S. Gurule, M. J. Reno, N. Ninad and E. Apablaza-Arancibia, "Evaluation of Photovoltaic Inverters Under Balanced and Unbalanced Voltage Phase Angle Jump Conditions", *47th IEEE Photovoltaic Specialists Conference (PVSC)*, 2020, pp. 1562-1569.

[12] R. Darbali-Zamora, N. S. Gurule, J. Hernandez-Alvidrez, S. Gonzalez and M. J. Reno, "Performance of a Grid-Forming Inverter Under Balanced and Unbalanced Voltage Phase Angle Jump Conditions", *IEEE 48th Photovoltaic Specialists Conference (PVSC)*, 2021.

[13] A. Yazdani and R. Iravani, "Voltage-Sourced Converters in Power Systems: Modeling, Control, and Applications", *Wiley-IEEE Press*, 2010, pp.1-541.

[14] M. Ebrahimi, S. A. Khajehoddin and M. Karimi-Ghartemani, "Fast and Robust Single-Phase DQ Current Controller for Smart Inverter Applications", *IEEE Transactions on Power Electronics*, vol. 31, no. 5, pp. 3968-3976, May 2016.

[15] V. Purba, S. V. Dhople, S. Jafarpour, F. Bullo and B. B. Johnson, "Reduced-order structure-preserving model for parallel-connected three-phase grid-tied inverters", *IEEE 18th Workshop on Control and Modeling for Power Electronics (COMPEL)*, 2017.

[16] W. Du, R. H. Lasseter and A. S. Khalsa, "Survivability of Autonomous Microgrid During Overload Events", *IEEE Transactions on Smart Grid*, vol. 10, no. 4, pp. 3515-3524, July 2019.

[17] W. Du and R. H. Lasseter, "Overload mitigation control of droop-controlled grid-forming sources in a microgrid", *IEEE Power & Energy Society General Meeting*, 2017, pp. 1-5.

[18] P. Piagi and R. H. Lasseter, "Autonomous control of microgrids", *2006 IEEE Power Engineering Society General Meeting*, 2006, pp. 1-8.

[19] M. E. Elkhatib, W. Du and R. H. Lasseter, "Evaluation of Inverter-based Grid Frequency Support using Frequency-Watt and Grid-Forming PV Inverters", *IEEE Power & Energy Society General Meeting (PESGM)*, 2018, pp. 1-5.